Ionic strength effects on the reactive uptake of ozone on aqueous pyruvic acid: Implications for air-sea ozone deposition

(Article begins on next page)

23 November 2024

Ionic strength effects on the reactive uptake of ozone on aqueous pyruvic acid: Implications for air-sea ozone deposition

Majda Mekic[1], Gwendal Loisel[1], Wentao Zhou[1], Bin Jiang[1], Davide Vione[2], Sasho Gligorovski[1,*]

[1] State Key Laboratory of Organic Geochemistry, Guangzhou Institute of Geochemistry, Chinese

Academy of Sciences, Guangzhou 510 640, China

[2] Dipartimento di Chimica, Università degli Studi di Torino, Via Pietro Giuria 5, 10125 Torino, Italy

Submitted to Environmental Science and Technology

*Corresponding author: gligorovski@gig.ac.cn

Abstract

A vertical wetted-wall flow tube technique was used to explore the ionic strength effects at the air-water interface in mediating the sea-surface reaction between ozone (O_3) and pyruvic acid (PA). The uptake coefficients of ozone on aqueous PA increase substantially with the concentrations of bromide (Br^-) ions, clearly indicating that the dry deposition of ozone could be significantly enhanced due to the presence of carbonyl compounds such as PA at the bromide-rich sea surface. Based on the observed uptake coefficients, the estimated deposition velocity of ozone (100 ppb) for a nM range of PA concentrations is $\sim 1 \cdot 10^{-3}$ m s^{-1}, which represents a significant contribution to the known deposition velocity of ozone at the sea surface.

The analysis of reaction products by Ultra-High Resolution Fourier Transform-Ion Cyclotron Resonance Mass Spectrometry suggests the formation of oligomers, during both the dark and light-induced heterogeneous reactions between gaseous O_3 and PA occurring at the surface of a dilute aqueous phase (representative of cloud droplets). The chemical structure of the detected high molecular weight compounds is much more complex than the oligomeric species identified during the photolytic degradation of bulk aqueous PA alone.

Introduction

The ocean-atmosphere interface represents the largest and most important interface on our planet, but at the same time it remains the biggest enigma for the scientific community [1]. The deposition of ozone to the ocean surface is a very important factor that controls the global ozone concentrations [2]. The dry deposition of ozone on the ocean surface is strongly depending on wind speed and turbulence, but it is also thought to have an important component arising from chemical reactions at the sea surface [3,4]. The reaction of I^- with ozone at the ocean surface (Chang et al., 2004) may also involve sea-salt aerosols and impact the global tropospheric ozone budget (Pillar et al., 2013). The estimated concentration decrease of ozone due to halogen chemistry is 4−6 ppbv over remote marine regions and over 6 ppbv in the coastal regions (Sarwar et al., 2015). The involvement of bromine atoms (Br), which have for instance enhanced measured values over the Dead Sea as a particular case, could also be an important ozone sink in some regions (Holla et al., 2015). Dead Sea water is in fact enriched in iodide, chloride and bromide. The number ratio I^-/Br^- in Dead Sea water is 1.2–4 times higher than in ocean water, and Br^-/Cl^- is at least 6.7 times higher than in ocean water. This implies that bromine and iodine chemistry could be of enhanced importance towards ozone deposition at the Dead Sea compared to open-sea conditions (Holla et al., 2015). The heterogeneous reaction of ozone with bromide ions at the ocean surface may increase the uptake of ozone, at the same time releasing photochemically active bromine compounds into the atmosphere [5-7]. These compounds can participate to the formation of secondary organic aerosols (SOA).

The reactive uptake of ozone by the organic compounds enriched at the sea-surface microlayer [8] can influence significantly the ozone budget in the marine boundary layer of the atmosphere. Although there is now growing understanding about the deposition velocities of ozone on the

ocean surface, the knowledge about the ozone's loss rate through its reactivity with the organic constituents of the coating material at the ocean surface remains uncertain.

The sea-surface microlayer, which is defined as the uppermost 1 μm to 1 mm of the ocean surface is enriched with organic compounds, mostly of biogenic nature [9]. Interestingly, when the sea surface is calm these compounds are more concentrated in the microlayer than in the subsurface water [9].

The α-keto acids such as pyruvic acid (PA) are widely spread at the ocean surface because they emerge from biological activity that is very active in the photic zone [10], as well as from non-biological decomposition of the hydroxylated amino acids [11]. Moreover, photochemical production by photodegradation of humic-like substances has been reported to be a key source of α-keto acids [10,12].

The observed vertical profiles of PA indicate concentrations of about 50 nmol L^{-1} at the ocean surface [11]. PA is a water-soluble compound, thus its apparent partition coefficient K has been reported to be $1.7 \cdot 10^5$ M atm^{-1} [13] and the net exchange direction is expected to be from air to sea. A value of 0.06 has been estimated for the reactive uptake coefficient of gaseous PA by water (Eugene et al., 2018). High concentrations of PA have also been detected in remote marine aerosols, for example over the North Pacific [14]. Long-term observations of dicarboxylic acids in the period 2001-2013 revealed a significant increase of PA concentrations in the marine aerosols over the North Pacific [15]. It is also expected that PA is photochemically active at the surface of atmospheric aerosol particles [Guzman et al., 2006a, Guzman et al., 2006b, Eugene and Guzman, 2017, Xia et al., 2018].

Bromide ions are ubiquitous in seawater with an average concentration of $8.6 \cdot 10^{-4}$ M, and their concentration is further enhanced in the nanolayer close to the air-sea interface (Carpenter and

Nightingale, 2015). The concentrations of bromide at the marine boundary layer, both in seawater and marine aerosols can reach levels of ca. 10 mM [Von Glasow et al., 2003].

Organic monolayers have been widely used in the past as a proxy to represent and resemble complex sea-surface microlayers [8, 19-25]. In this study we used aqueous PA as an important atmospheric component, as well as a proxy of dicarboxylic acids. Indeed, while being a monocarboxylic compound, PA shares some volatility/partitioning properties of dicarboxylic acids due to the additional polarity provided by the carbonyl group. Here we examined the role that organic surface films made up of aqueous PA may play in controlling the ozone deposition velocity. To do so, we measured the uptake of gas-phase ozone on aqueous PA. Because PA is known to be a photochemically active compound in the actinic region of the solar spectrum [Guzman et al., 2006a, Guzman et al., 2006b, Eugene and Guzman, 2017, Xia et al., 2018, Grgic et al., 2010, Gomez Alvarez et al., 2012], the reactive uptakes of ozone were examined under both dark conditions and light irradiation. Considering that ionic strength effects can play a significant role in the photochemical activity of PA [35, Rincon et al., 2010], we have evaluated the uptake coefficients of gaseous ozone on aqueous PA as a function of different bromide concentrations.

Finally, the oligomeric species formed in the heterogeneous reaction of ozone with aqueous PA in the dark and under light irradiation were evaluated by the means of Ultrahigh-Resolution Electrospray Ionization Fourier Transform Ion Cyclotron Resonance Mass Spectrometry (FT-ICR MS).

Materials and Methods

The production of ozone was achieved by a commercial ozone generator (UVP, LLC Upland, UK), which is based on O_2 photolysis by a mercury penray lamp inserted into the radiation housing. For this purpose, 200 mL min^{-1} (range 0-500 mL min^{-1}, Sevenstar CS200 mass flow controller; accuracy, ±1%) of pure oxygen (O_2, purity 99.999% Guangzhou Kehanda Trading, China) flows through the ozone generator. The ozone thus obtained is injected through a mobile injector, which also allows for varying the liquid surface in contact with O_3 for kinetic studies. The gas outlet of the flow tube (for details about the flow-tube reactor see section VWWFT) is diluted with a flow of air-carrier gas (purity 99.999% Guangzhou Kehanda Trading, China) at 1.3 L min^{-1} (range 0-2 L min^{-1}, Sevenstar CS200 mass flow controller; accuracy, ±1%), for a total flow of 1.5 L min^{-1} that is needed to feed the ozone analyzer (Thermo Scientific Model 49i, USA) in order to determine the ozone concentration.

PA (98 %) and sodium bromide (≥ 98 %) were used as obtained from Sigma-Aldrich, without any further purification. All solutions were prepared in Milli-Q quality water provided by Sartorius (18 M-ohm, H_2O-MM-UV-T, Germany).

In the experiments with NaBr the pH varied in the range between 6.57 and 7.17. We avoided the addition of further components to correct pH, in order to avoid the interferences that can be caused by such additions.

Fourier Transform-Ion Cyclotron Resonance Mass Spectrometry (FT-ICR MS)

The aqueous samples were analyzed with a solariX XR FT-ICR MS instrument (Bruker Daltonik GmbH, Bremen, Germany) equipped with a refrigerated, 9.4 T actively shielded superconducting magnet (Bruker Biospin, Wissembourg, France) and a Paracell analyzer cell. The samples were

analyzed by FT-ICR MS immediately after the reaction. The ionization of the samples was performed in the negative ion mode using an ESI ion source (Bruker Daltonik GmbH, Bremen, Germany). The detection mass range was set to m/z 150 – 1000. Ion accumulation time was set to 0.65 s. A total of 64 continuous 4M data FT-ICR transients were co-added to enhance the signal-to-noise ratio and dynamic range. The mass spectra were calibrated externally with arginine clusters in the negative ion mode, using a linear calibration. The final spectrum was internally recalibrated with typical O_2 class species peaks using quadratic calibration in DataAnalysis 4.4 (Bruker Daltonics). A typical mass-resolving power (m/Δm50%, in which Δm50% is the magnitude of the mass spectral peak full width at half-maximum peak height) >450 000 was achieved at m/z 319, with <0.3 ppm absolute mass error.

The custom software was used to calculate all mathematically possible formulas for all ions with a signal-to-noise ratio above 10, using a mass tolerance of ±1ppm. Peaks that were present in blank samples with an average S/N > 20 were removed from all the samples. The maximum number of atoms for the formula calculator was set to: 30 ^{12}C, 60 ^{1}H, 20 ^{16}O, 3 ^{14}N, 1 ^{32}S, 1 ^{13}C, 1 ^{18}O and 1 ^{34}S. The identified formulas containing isotopomers (i.e., ^{13}C, ^{18}O or ^{34}S) are not discussed here. For the chemical formula $C_cH_hO_oN_nS_s$, the double bond equivalent (DBE) is calculated using the following equation: DBE = (2c+2−h+n)/2. The details of data processing were described previously [36, 37].

Vertical wetted wall flow tube (VWWFT)

The VWWFT was used to investigate the heterogeneous reaction between the gas-phase ozone and the liquid phase, which consisted of an aqueous solution containing PA and a mixture of PA and NaBr in different experiments, under well-defined conditions. The flow tube is a Borosilicate glass cylinder, with height of 90 cm and an inner diameter of 0.9 cm. The flow tube reactor was thermostated using a circulating water bath through the outer jacket, and temperature control was obtained with a Lauda (Germany) RC6 refrigerated bath with RCS thermostat. The temperature accuracy was ±0.02K at 293 K. The thermostated bath was started two hours before the experiments to achieve stable surface temperature conditions.

A peristaltic pump (LabV1/MC4, SHENCHEN, China) was used to draw a constant flow of a freshly prepared solution containing aqueous PA or a mixture of PA and dissolved NaBr onto the top of the flow tube. The solution flowed downward on the inner walls of the tube as a homogenous and uniform liquid film, completely covering the tube inner walls. At the bottom of the tube the reacted solution was sent to the waste or to a sample vial for further analysis by pH meter, UV-VIS spectrophotometer, and FT-ICR MS.

The thickness of the liquid film flowing on the tube walls was estimated as follows [38]:

$$f = \left(\left[\frac{3\mu v}{2r\pi g \rho}\right]\right)^{1/3}$$

Eq-1

where μ is the viscosity [cP, where 1 cP = 1 mPa s], v the liquid flow-rate [cm^3 s^{-1}], r = 0.45 cm the inner radius of the tube, g = 981 cm s^{-2} the gravitational acceleration, and ρ the density of the liquid [g cm^{-3}]. Under the experimental conditions of this study the thickness of the film was 0.024 cm. The velocity of the film u at any depth x beneath the surface is expressed with the following equation [38]:

$$u = \frac{3}{2\left(\left[\frac{\nu}{2\pi r}\right]\right)^{2/3}\left(\left[\frac{g\rho}{3\mu}\right]\right)^{1/3}\left[1 - \left(\left[\frac{x}{f}\right]\right)^2\right]}$$

Eq-2

Under our experimental conditions the surface ($x = 0$) velocity in the gas-liquid interaction zone was 1.84 cm s^{-1}. The film was perfectly uniform without any ripples, flowing on the glass surface under laminar conditions because the Reynolds number (R_e) [39] was smaller than 10 (R_e = 0.2):

$$R_\varrho = \frac{\nu\rho}{2\pi r\mu}$$

Eq-3

The gaseous O_3 was introduced into the reactor from the upper side via a movable injector made out of Borosilicate glass. This set-up implies that both the gas-phase ozone and the liquid film flow in the same direction. To convert the reaction length into contact time, it is necessary to know the gas flow velocity inside the flow tube. The gaseous ozone was introduced into the reactor with a flow rate of 200 mL min^{-1}, which leads to an average speed of 5 cm s^{-1} in the reactor. By varying the position of the injector inside the reactor it is possible to control the contact time between the gaseous O_3 and the liquid surface, which allows for the reaction kinetics to be elucidated.

Results and Discussion

Kinetic data treatment

The reactive uptake of O_3 into a liquid is characterized by: i) mass transfer from the gas phase to the aqueous phase, described by the diffusion coefficient of O_3 in the gas phase, D_{gas}; ii) mass accommodation (α), defined as the fraction of collisions of O_3 with the liquid surface that can lead to incorporation of O_3 into the bulk; iii) diffusion of O_3 into the aqueous phase,

characterized by the diffusion coefficient of O_3 (D_{liq}), and iv) liquid-phase reaction, characterized by the second-order rate constant for the bimolecular reaction between O_3 and PA (k_{2nd}) [40]. The reactive uptake coefficients were estimated by measuring the loss rate of gaseous ozone flowing along the vertically aligned flow tube. Under these conditions only the heterogeneous reaction between the gas-phase ozone and the liquid film occurs, which is described with a first-order rate law with respect to the gas-phase concentration of ozone:

$$\frac{c_i}{c_0} = e^{(-kt)}$$

Eq-4

where k is the first-order rate constant for the reaction of gas-phase ozone with the liquid film containing PA and/or NaBr, and t is the residence time of ozone in the reactor.

Figure 1 shows the first-order ozone decay on a liquid film consisting of aqueous PA under different experimental conditions, as a function of the residence time of O_3 in the flow tube reactor. First of all, note that negligible ozone consumption was observed without PA and Br$^-$ (data not shown), which means that no ozone photolysis was operational in our system (is also means that no $^\bullet$OH could be produced upon ozone photolysis). It is then shown in the Figure that the uptake coefficient of ozone in the presence of PA and Br$^-$ under light irradiation ($\gamma = 1.5 \cdot 10^{-7}$) was enhanced compared to that seen in the dark ($\gamma = 5.7 \cdot 10^{-8}$). In contrast, the ozone uptake coefficients on aqueous PA in the absence of bromide ions had almost identical values under both dark and light conditions. These results indicate that PA in the presence of elevated concentrations of bromide ions introduces a new, light-enhanced reaction mechanism on the water surface that increases the uptake of ozone (section Reaction Mechanism, *vide infra*).
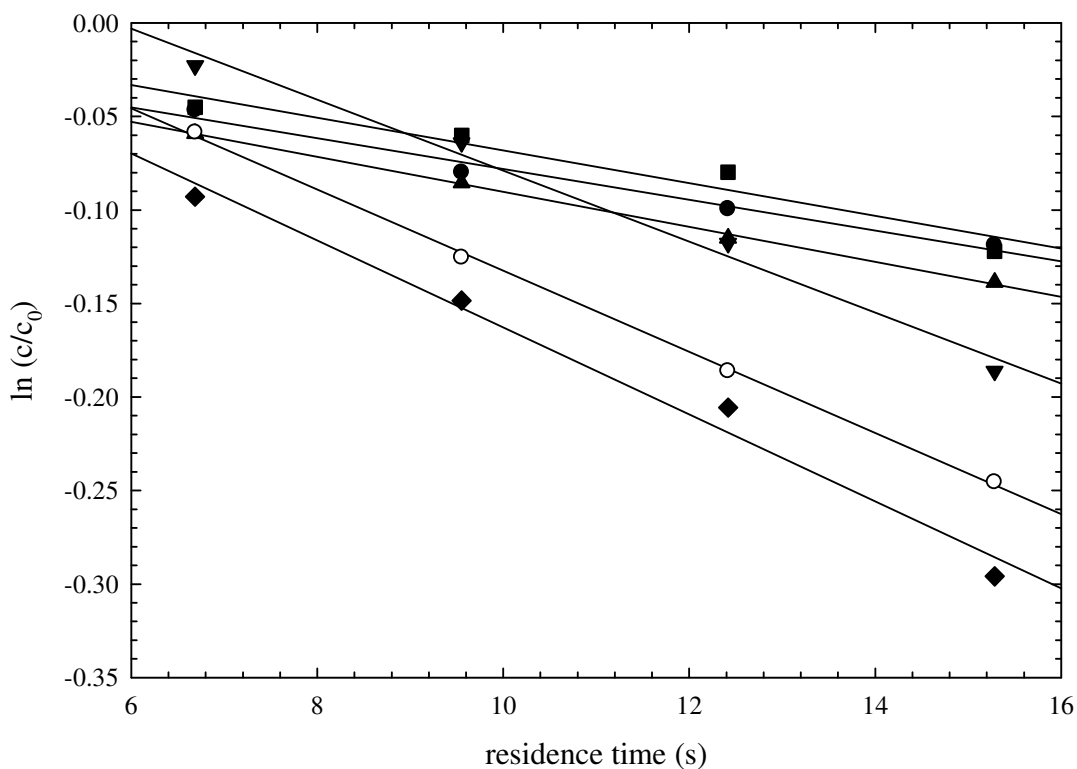
Figure 1: First-order decay of ozone on aqueous PA ([PA] = 5 · 10^{-4} mol L^{-1}): ●) dark reaction, ▲) under light irradiation, ■) mixed with bromide ions in the dark, ♦) mixed with bromide ions under light irradiation. First-order decay of O_3 on bromide ions without PA: ▼) in the dark, and ○) under light irradiation. When applicable, it was [NaBr] = 0.05 mol L^{-1}.

For slow aqueous-phase reactions, the diffusion phenomena can be neglected in kinetic data treatment because they are faster than the reactions; indeed, the rate-determining step of the overall process is reaction instead of diffusion. In this case the first-order loss rate of gas-phase ozone is given as follows [20]:

Eq-5

where $[O_3^g]$ and $[O_3^{aq}]$ are the concentrations of ozone in the gas phase and in the aqueous phase, respectively, [PA] is the concentration of PA in the aqueous phase, k_{2nd} is the second-order rate constant between O_3 and PA in the aqueous phase, H_{O3} is the Henry's law constant of O_3 in the dilute aqueous phase ($H_{O_3} = 1.13 \cdot 10^{-2}$ (M atm^{-1})) [41], r is the internal radius of the flow tube (r = 0.45 cm), and $\bar{\upsilon}$ is the mean molecular velocity of gas-phase ozone. The latter can be calculated from the collision theory [42] as follows:

$$\bar{\upsilon} = \sqrt{\frac{8\,R\,T}{\pi\,M}}$$

Eq-6

where R is the gas constant (R= 0.082 (L atm K^{-1} mol^{-1})), T (K) is the gas-phase temperature, and M is the molar mass of O_3 (M= 48 g mol^{-1}). The mean molecular velocity of gaseous ozone was calculated as $\bar{\upsilon} = 35\,900$ cm s^{-1} at 298 K.

The pseudo first-order rate constant k_{1st} of ozone in the aqueous phase is obtained from Eq-5 as follows:

Eq-7

and the uptake coefficient of gas-phase ozone on aqueous PA can be calculated as follows [20]:

$$\gamma = \frac{2\,k_{1st}\,H_{O_3}\,R\,T\,r}{\bar{\upsilon}}$$

Eq-8

In this case the measured uptake coefficients are linearly proportional to the concentration of aqueous PA:

$$\gamma = \frac{2\,k_{2nd}\,H_{O_3}\,R\,T\,r\,[PA]}{\bar{v}}$$

Eq-9

However, Eq-9 may not be valid when the diffusion phenomena play a role, i.e., when radial gas concentration profiles build up [21, 43]. In previous studies the Cooney-Kim-Davis equation [44] was applied as described in detail by Behnke et al. (1997) [43] to account for gas-phase diffusion phenomena. In this case the uptake coefficient is given by the following equation:

Eq-10

Considering that $k_{1st} = k_{2nd}[PA]$, Eq-10 becomes:

Eq-11

where D_{aq} is the diffusion coefficient of O_3 in the dilute aqueous phase (D_{aq} = 1.176 · 10^{-5} (cm^2 s^{-1})) [41].

The diffuso-reactive length (l) is a measure of the distance from the interface in which the reaction occurs [40]:

$$l = \sqrt{\frac{D_{aq}}{k_d}}$$

Eq-12

This length can be compared to the thickness d of the reactant film containing PA in the flow tube. The value of d is given as follows [20]:

$$d = \frac{F_{aq}\,t}{S}$$

Eq-13

where F_{aq} is the flow of the reactant solution (F_{aq} = 0.083 cm^3 s^{-1}), t (s) is the residence time of the aqueous film in the flow tube and S is the surface of the flow tube (S = 255 cm^2). For an

average time of 10 s, the thickness of the aqueous film is calculated as d = 3.27 · 10^{-3} cm. The lower limit of the pseudo-first order rate constant can then be calculated from Eq-12, as follows:

$$k_d = \frac{D_{aq}}{l^2} \leq \frac{D_{aq}}{d^2}$$ Eq-14

Under our experimental conditions it was k_d = 1.65 s^{-1}, implying that above this value the chemical reaction is diffusion-limited because the diffusion rate becomes lower than the reaction rate.

For low values of the uptake coefficients as those determined in this study, which ranged from 5 · 10^{-8} to 1 · 10^{-6}, Eq-8 is fully justified implying that the diffusion processes cannot affect the uptake coefficients of ozone. Hence, it can be reasonable to conclude that the reaction is mainly confined to the surface region at an atmospherically relevant ozone mixing ratio (100 ppb) (*vide-infra*).

Ionic strength effects on the uptake coefficients

The salinity of the ocean is an important parameter that changes as a function of the balance between evaporation and precipitation, as well as the extent of mixing between the sea surface and deeper waters [45].

In sea-salt particles, the ionic strength is an important parameter because each ion is surrounded by an extended solvation shell affecting the reaction rates [46]. The high concentrations of ions in solutions of high ionic strength such as the sea-surface microlayer and the sea-salt aerosol particles can alter the solubility of ozone (Pillar et al., 2013). In this case, the Henry's law constant (H_o) of ozone used in the dilute aqueous phase must be modified by using the Setchenow equation, to take the effect of ionic strength into account.

Setschenow [47] established an empirical equation that describes quantitatively the effect of added salt, NaBr in this case:

$$\log\left[\left(\frac{H}{H_0}\right)\right] = K_s c_s$$

Eq-15

where H is the Henry's law constant of ozone for the salt solution, K_s is the Setschenow's constant, which is a theoretically significant salt parameter, and c_s is the concentration of NaBr (mol L^{-1}). Rischbieter et al. [48] developed a theoretical model to estimate the Henry's constants of ozone for pure water (H_0) in the temperature range 273-333 K, correct within a mean error of ± 10%, as follows:

$$\log(H_0[kPa\ m^3\ mol^{-1}]) = 5.12 - \frac{1230}{T[K]}$$

Eq-16

An empirical model that combines the individual effects of the used salt ions and gas on K_s was suggested by Schumpe [49]:

$$K_s = \sum_i (h_i + h_G)x_i$$

Eq-17

where h_i and h_G are the contributions of the used ions and gas. The parameter x_i expresses the stoichiometry number of the ion i in the chemical formula of the used salt (e.g., for NaBr one has $x(Na^+) = 1$ and $x(Br^-) = 1$). Later, Weisenberger and Schumpe [50] suggested an equation that describes the temperature dependence of the gas-specific parameter h_G in Eq-17:

$$h_G = h_{G,0} + h_T(T - 298.15K)$$

Eq-18

where $h_{G,0}$ and h_T are specific parameters for the dissolved gas, O_3 in this case. The overall equation to calculate the Setschenow's constant, K_S, turns into the following:

$$K_s = \sum_i (h_i + h_{G,0} + h_T(T - 298.15K))x_i$$

Eq-19

The values of h_i, $h_{G,0}$ and h_T for various ions and gases in a wide temperature range are summarized by Beltran, (2004) [51]. The contributions of the ions used in our calculations were $h_i(Na^+) = 0.1143$ m^3 kmol^{-1} and $h_i(Br^-) = 0.0269$ m^3 kmol^{-1}, while the gas specific model parameters for ozone were $h_{G,0} = 3.96 \cdot 10^{-3}$ m^3 kmol^{-1} and $h_T = 1.79 \cdot 10^{-3}$ m^3 kmol^{-1}, respectively.

Finally, for the estimation of the Henry's law constants of gases in aqueous salt solutions, the Eq-15 gets modified as follows:

$$\log\left(\frac{H}{H_0}\right) = \sum_i [(h)_i + h_{G,0} + h_T(T - 298.15K)]c_s$$

Eq-20

The calculated Henry's law constants of ozone at different salt concentrations are summarized in Table 1.

Table 1: Calculated Henry's law constants of ozone in the presence of different salt concentrations

[NaBr] (mol L^{-1})	H (kPa m^3 mol^{-1})	H (dimensionless) RT
$5 \cdot 10^{-1}$	10.854	0.227
$3 \cdot 10^{-1}$	10.167	0.242
$1 \cdot 10^{-1}$	9.523	0.258
$5 \cdot 10^{-2}$	9.369	0.263
$1 \cdot 10^{-2}$	9.247	0.266
$5 \cdot 10^{-4}$	9.219	0.267

Previously we have shown that the ionic strength has an impact on the photolytic loss rate of PA in the aqueous phase [35], and that the first-order photoinduced decay rate constant of PA increased by ca. 3 times at elevated ionic strength. The observed effects of increasing rate constants with increasing ionic strength during the reactions between atmospherically relevant oxidant species ($^\bullet NO_3$, $^\bullet OH$, $Cl^\bullet$, and $Cl_2^{\bullet -}$) and organics have been previously reported and summarized in a review article by Herrmann [46].

To shed some light on the influence of Br^- on the reactivity of PA towards ozone, we performed a set of experiments to evaluate the effect of the ionic strength on the heterogeneous reaction between gas-phase ozone and the aqueous film of PA. The dependence of the uptake coefficients of ozone (100 ppb) on an aqueous film having $[PA] = 5 \cdot 10^{-4}$ mol L^{-1}, as a function of Br^- concentrations ranging between $5 \cdot 10^{-3}$ and 0.5 mol L^{-1} was evaluated under dark conditions and in the presence of light (Figure 2).

At low O_3 concentrations the surface reaction dominates, as can be seen in Figure 2S (see the supplementary information). The tendency of ozone to be enriched at the interface is likely due to the combination of its relatively low solubility in water with a substantial polarizability (2.85 Å^3), so that the van der Waals interactions between O_3 and H_2O at the interface become important [5]. The theoretical calculation performed by Hunt et al. [5] gave evidence of a surface enhancement of Br^- ions accompanied by a spatial separation of the positively and negatively charged ions in the interfacial region. The enrichment of halide anions such as Br- at the air-water interface was also experimentally confirmed by help of ESI-MS and atomic force microscopy (Guzman et al., 2012, Lee et al., 2017).
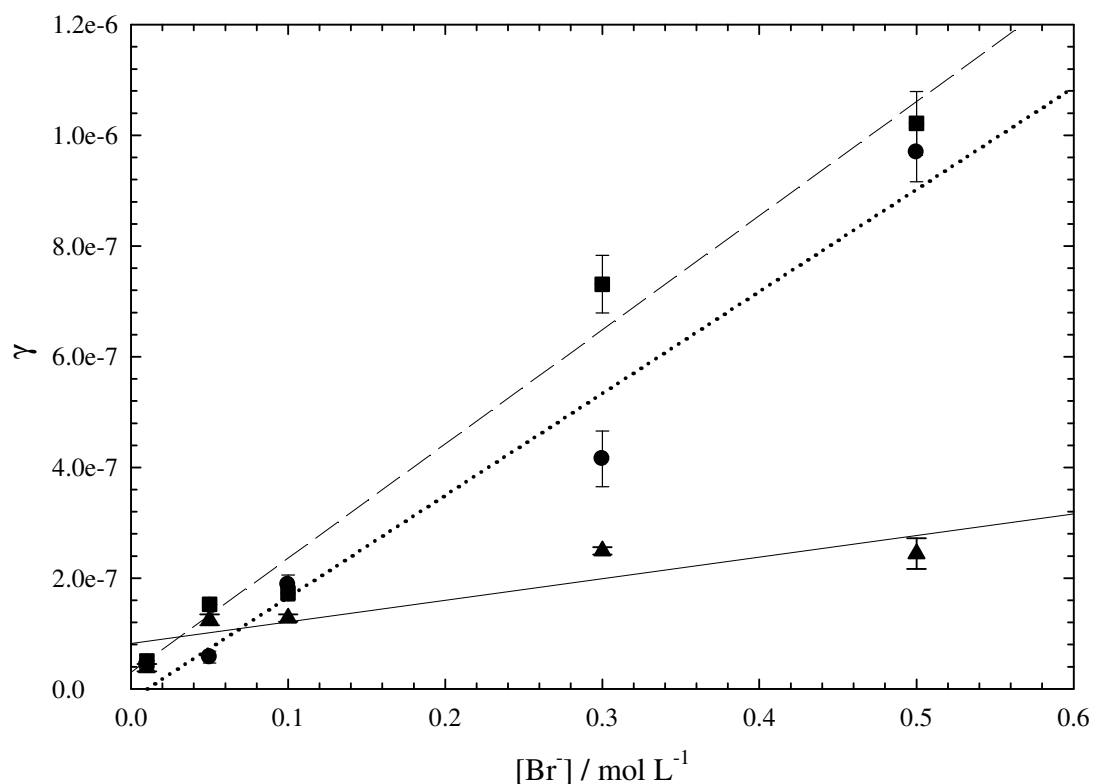
Figure 2: Uptake coefficients of ozone (100 ppb) as a function of the Br^- concentration. ▲) Neat Br^- solution in the dark; ●) PA + Br^- in the dark, ■) PA + Br^- under irradiation. [PA] $= 5 \cdot 10^{-4}$ mol L^{-1}. The solid line is the regression for the uptake coefficients on a neat Br^- solution in the dark; the dotted line represents the regression line for the uptake coefficients on a mixture of PA and bromide ions in the dark; the long dashed line is the regression for the uptake coefficients on a mixture of PA and Br^- under irradiation. The error bars represent 2σ, derived from the statistical error of the slope of the plot of ln (c/c_0) versus the residence time.

The obtained uptake coefficients of ozone on a neat NaBr solution in the dark range from $1.25 \cdot 10^{-7}$ at $[Br^-] = 5 \cdot 10^{-2}$ mol L^{-1} to $2.44 \cdot 10^{-7}$ at $[Br^-] = 5 \cdot 10^{-1}$ mol L^{-1}. Our findings are in good agreement with the uptake coefficient of ozone ($\sim 10^{-7}$) on $5 \cdot 10^{-2}$ mol L^{-1} Br^- measured by Clifford et al., 2008 [8], and with the uptake coefficients of ozone ($1.4 \cdot 10^{-7}$ on $8.5 \cdot 10^{-3}$

mol L^{-1} Br$^-$, and $2.7 \cdot 10^{-7}$ on $8.5 \cdot 10^{-2}$ mol L^{-1} Br$^-$) obtained in the study of Oldridge and Abbatt, 2011 [7]. From Figure 2 it can be seen that there is a relatively weak dependence between the uptake coefficients of O_3 and the concentration of Br$^-$ in the absence of PA. This result is in agreement with the theoretical calculations of the O_3 interaction with water and a NaBr salt solution, in which the effect of the dissolved salt on the trapping of O_3 was small compared to neat water [5]. However, the slope of the plot depicting the uptake coefficients of O_3 vs. [Br$^-$] is substantially higher in the presence of PA ($1.8 \cdot 10^{-6}$) compared to a neat Br$^-$ solution ($3.0 \cdot 10^{-7}$). PA is highly soluble, and it will partition completely into cloud water, in the atmospheric aerosols and in the ocean [13]. However, dissolved salts reduce the solubility of PA in the aqueous phase and enhance the PA concentration at the surface due to the salting-out effect. This could be a possible reason for the enhanced uptake coefficients of ozone on bromide ions in the presence of PA (but see also the later section on the possible reaction mechanisms). The slope of γ vs. [Br$^-$] increased even more upon irradiation of an aqueous film composed of a mixture of PA and Br$^-$. This issue clearly indicates that the dry deposition of ozone to the sea surface could be significantly enhanced by carbonyl compounds (e.g., pyruvic acid) that occur in the sea-surface microlayer. Because of the irradiation effect, the increase of the ozone deposition to the sea surface would be higher during the day than at night.

Possible reaction mechanisms

Carbonyl compounds such as PA are known because of their photosensitizing properties [28, 29, Carlton et al., 2006, Guzman et al., 2006, Eugene and Guzman, 2017, Xia et al., 2018, Altieri et al., 2006]. Although these compounds are often called photosensitizers only in relation to their

ability to produce singlet oxygen, they are actually capable of bringing about indirect photolysis by several mechanisms [29, 52].

The excited triplet state of PA can initiate free-radical reactions [32], and this mechanism is responsible for the enhanced decomposition of dissolved organic compounds in the atmospheric aqueous phase and in the ocean. Moreover, PA is actually able to react with O_3 in the bulk aqueous phase under dark conditions, with a second-order reaction rate constant in the range of 0.1-1 L mol^{-1} s^{-1} depending on pH [53].

In the presence of elevated concentrations of bromide, the uptake of ozone on aqueous PA increases drastically over that seen on pure water (**Figure 2**), indicating that salts exhibit a strong influence on the reaction. Because the reaction between O_3 and Br$^-$ is not responsible for the enhanced uptake of ozone [8], it can be suggested that the surface concentration of PA is higher in the aqueous film containing Br$^-$ ions due to a salting-out effect. This phenomenon increases the reaction rate between PA and O_3 and, therefore, the uptake of ozone at low ozone concentrations (100 ppb) where the surface reaction dominates.

Another possibility is that PA interferes with the reaction between Br$^-$ and O_3, which initially follows a pre-equilibrium step before evolving into the products [54]. If PA is able to react with the reaction intermediate BrOOO$^-$ (Artiglia et al., 2017), this process could account as well for the enhanced O_3 uptake in the presence of PA and Br$^-$.

$$Br^- + O_3 \leftrightarrows BrOOO^- \qquad\qquad\qquad \text{R-1}$$

$$BrOOO^- \rightarrow BrO^- + O_2 \qquad\qquad\qquad \text{R-2}$$

$$BrOOO^- + PA \rightarrow Products \qquad\qquad\qquad \text{R-3}$$

Finally, the further enhancement observed with PA + Br$^-$ under irradiation compared to the same system in the dark can be accounted for by a process photosensitized by the PA triplet state

(^{3}PA*). As similar behaviour has for instance been reported in the case of O_3 and chlorophyll under irradiation [55].

$$PA + h\nu \rightarrow {}^1PA* \xrightarrow{ISC} {}^3PA* \qquad\qquad R\text{-}4$$

$$^3PA* + O_3 \rightarrow PA^{\bullet+} + O_3^{\bullet-} \qquad\qquad R\text{-}5$$

In analogy with the mechanism suggested by Jamoul et al. (2009), the photoexcited ^{3}PA* may form a contact complex with a bromide ion, then an ion pair via intramolecular electron transfer:

$$^3PA* + Br^- \leftrightarrows {}^3PA*\cdots Br^- \leftrightarrows [PA^\bullet\text{-}O^-\cdots Br^\bullet]*$$

The formation of such complex is thermodinamically favorable for Br^- and unfavorable for I^- (Jamoul et al., 2009). The interaction of ozone with the formed charge-transfer complex can be the reason for the enhanced uptake coefficients in the presence of light.

Molecular composition of the products by high-resolution mass spectrometry

Thanks to ultrahigh resolution and ppb mass accuracy of the spectra, FT-ICR MS provides a confident assignment of the unique elemental composition for each mass-spectrum peak [56]. FT-ICR MS is one of the most powerful tools that can be used for the characterization of complex organic compounds in atmospheric aerosols at the molecular level [37]. Typically, a FT-ICR MS instrument is tuned to detect and identify the chemical composition of large molecular-weight compounds with m/z > 150 Da. It has been demonstrated that the iso-abundance plots of DBE versus carbon numbers allow for the differentiation of complex organic mixtures based on the chemical composition [36]. The iso-abundance plot of DBE *versus* carbon numbers for the detected $C_xH_yO_z$ species produced by the dark heterogeneous reaction of ozone with aqueous PA is presented in **Figure 3**.

The DBE parameter represents the number of double bonds plus rings characterized as unsaturations occurring in the organic compounds. In this case, the term unsaturation corresponds to a double bond. **Figure 3** shows the increase of DBE with the carbon atoms in the molecule, and it indicates that most of the $C_xH_yO_z$ products formed upon dark reaction between gas-phase O_3 and the aqueous film of PA have DBE values in the range between 2 and 10, with 6-18 carbon atoms and 5-8 oxygen atoms. To fulfill these conditions the compounds should have 2-6 carbonyl groups, and the remaining oxygen atoms (if any) might be included in functional groups such as hydroxyl or carboxyl.
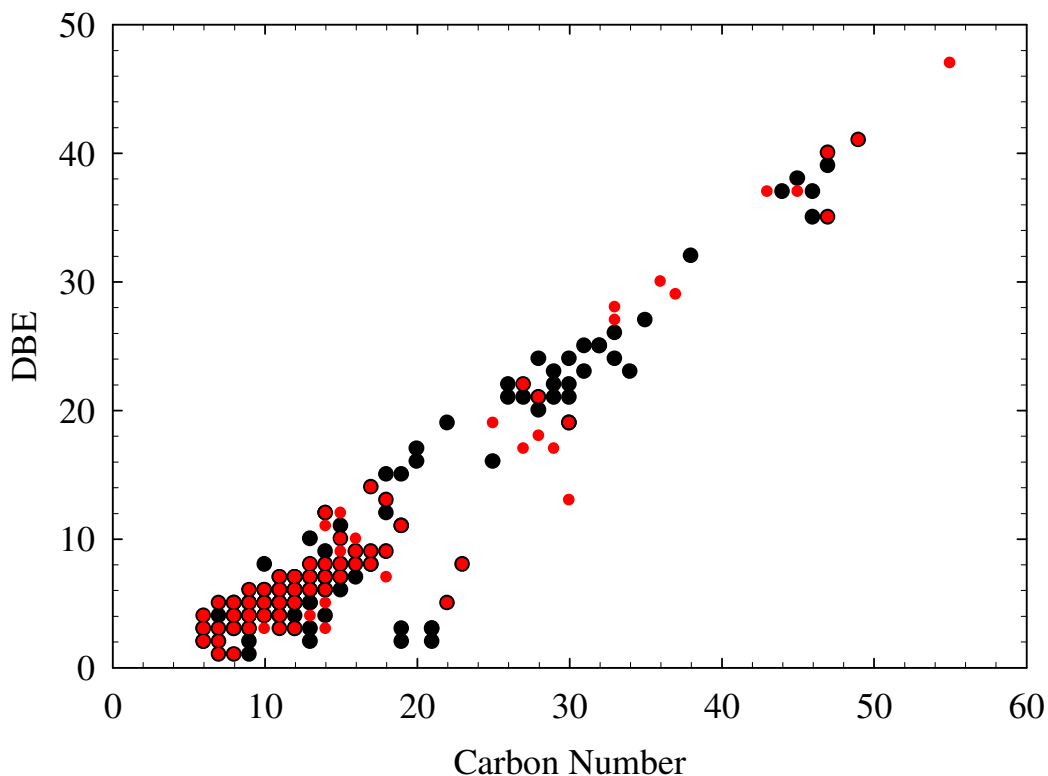
Figure 3: Iso-abundance plot of DBE *versus* carbon numbers for the $C_xH_yO_z$ species detected upon: ●) dark heterogeneous reaction between O_3 and aqueous PA, and ●) light-induced heterogeneous reaction between O_3 and aqueous PA

Figure 4A shows the mass spectrum of the organic compounds formed upon reaction of ozone ($[O_3]$ = 2.46 · 10^{12} molecules cm^{-3}) and pyruvic acid ($[PA]$ = 5 · 10^{-3} mol L^{-1}) at the water surface in the dark. The most abundant peaks appearing during the dark heterogeneous reaction of gaseous ozone with aqueous PA were $C_6H_5O_5^-$, $C_6H_7O_6^-$, $C_7H_9O_6^-$, $C_7H_{11}O_7^-$, $C_9H_9O_8^-$, $C_{15}H_{17}O_{25}^-$, $C_{29}H_{15}O_{24}^-$, $C_{47}H_{15}O_{12}^-$, $C_{30}H_{19}O_{25}^-$, and $C_{47}H_{25}O_{13}^-$. Among the ions showing elevated intensity, $C_{47}H_{25}O_{13}^-$ has the largest molecular weight (797.1301 Da) and a DBE value of 35.

Figure 4B depicts the high molecular-weight (oligomeric) compounds formed upon light-induced heterogeneous reaction of O_3 with aqueous PA. The chemical structure of the formed oligomers differs from those produced during the dark reaction, because the most abundant peaks are found in the range between 150 and 350 Da. There are some common peaks between the dark and light experiments and, when this happens, the peaks found under irradiation have higher intensity (Figure 4A and 4B). Compared to the dark reaction, there are two new peaks corresponding to $C_{13}H_{15}O_{11}^-$ (m/z 347.0621) and $C_{33}H_{11}O_9^-$ (m/z 551.0414) that appeared during the light-induced process. In the presence of light, the peak having the largest molecular weight (551.0414 Da) among those with significant abundance is $C_{33}H_{11}O_9^-$. Higher-mass oligomers (up to 800 Da) were identified during the dark reaction (Figure 4A), but they are most probably fragmented under irradiation.

A number of studies have shown that the aqueous chemistry of PA is characterized by the formation of oligomers, under both light and dark conditions [28, 31, 32, 34]. However, a comparison between the previous results and the present ones suggests that the products formed from the reaction of O_3 with PA at the water surface (at low ionic strength, which under

environmental conditions could be the surface of cloud droplets and aerosol deliquescent particles), either in the dark or under irradiation exhibit much more complex structure than the products formed upon photolytic degradation of PA alone in the bulk aqueous phase.

A recent study has reported different kinds of products formed during the photochemical degradation of PA in the bulk and at the air-liquid interface (Fu et al., 2018). These authors demonstrated that higher molecular weight compounds are formed at the air-liquid interface as a result of radical-radical reactions, compared to the compounds formed in the bulk that mainly derive from decarboxylation, esterification and anhydride reactions. The formation of oligomeric species such as those detected in the present study would influence the mass transfer of gas-phase compounds within the cloud droplets and aerosol deliquescent particles. Details on product formation and plausible reaction pathways describing the formation of oligomers are out of the scope of this study.
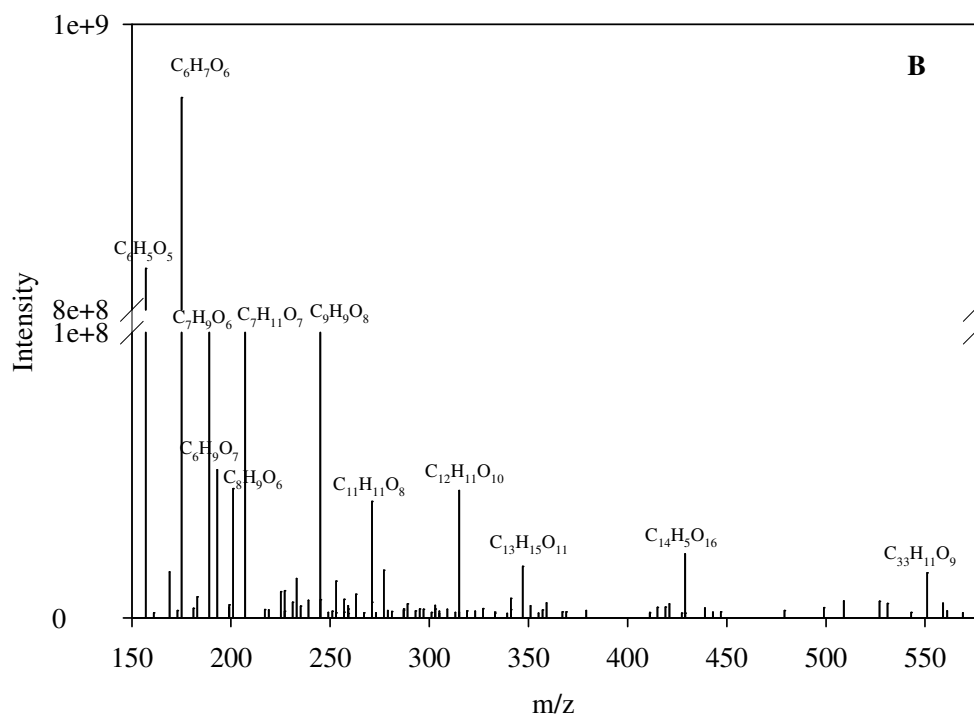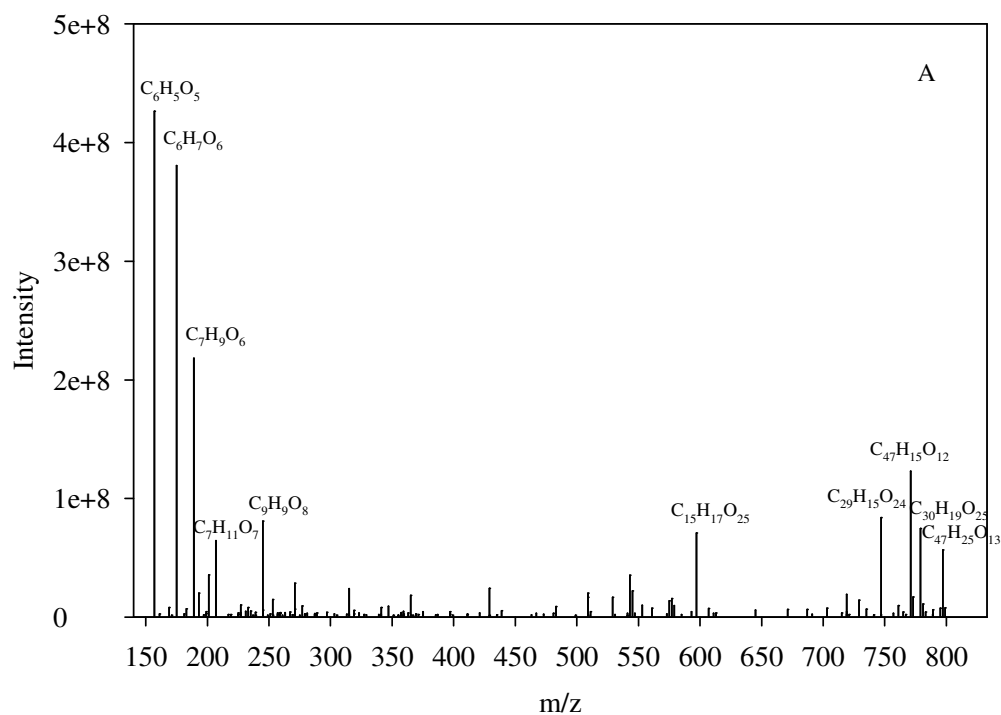
Figure 4: Relative abundances scanned in negative mode by FT-ICR MS of the species produced by the heterogeneous reaction of O_3 with aqueous PA, **(A)** under dark conditions and **(B)** under irradiation.

Atmospheric Implications

Ozone exhibits the third largest global warming effect after CO_2 and CH_4; hence, it plays an important role in the climate system [57]. The ozone lost by dry deposition on the ocean surface was estimated to be approximately one third of the ozone lost by photochemical decomposition in the marine boundary layer of the South Atlantic [58]. Considering that the oceanic concentrations of PA are about 50 nM at the surface [11] and that the concentrations of bromide in the marine boundary layer (in both seawater and marine aerosols) can reach levels of ca. 10 mM [19 and references therein], we can roughly estimate the deposition velocities of ozone on the ocean surface due to the chemical reactivity with dicarboxylic acids such as PA.

The concentrations of reactive halogen species in the surface microlayer are higher compared to their concentrations in the bulk, due to the reactions of their precursors with the atmospheric oxidants that are being deposited on the water surface [9]. The main sources of reactive halogen species are in fact the heterogeneous reactions of O_3 undergoing deposition at the surface with I^- [59] and Br^- [7], to produce reactive intermediates such as, respectively, I_2/HOI and HOBr/Br_2 (Pillar et al., 2013). The chemical loss of ozone due to its surface reaction with I^- was considered to be the most important contribution to the dry deposition of ozone itself at the ocean surface. The ozone deposition velocities due to its surface reactivity with I^- were reported to be in the range of 0.021-$1.9 \cdot 10^{-4}$ m s^{-1}, depending on the concentration of iodide species [60]. For iodide concentrations in the range between 50 and 200 nM the deposition velocity of ozone varied between $5.0 \cdot 10^{-5}$ and $1.0 \cdot 10^{-4}$ m s^{-1} [60]. Moreover, Martino et al. [60] reported a deposition velocity of ozone of $1.2 \cdot 10^{-4}$ m s^{-1} due to the reaction with a mixture of DOM and iodide at typical oceanic concentrations of 150 nM iodide and 2 mg L^{-1} DOM. These values are

comparable with the deposition velocities in the range of 10^{-5}–10^{-3} m s^{-1} estimated by Clifford et al. [8], based on the measured uptake coefficients of gaseous ozone on a liquid film made up of chlorophyll.

We have shown here that at low ozone concentrations the surface component of the reaction between O_3 and PA dominates over that in the bulk. At an atmospherically relevant ozone mixing ratio (100 ppb) [61], the reactive uptake coefficient of O_3 on aqueous PA in the presence of bromide ions (5mM) can be extrapolated from the intercept of the linear regression of the measured uptake coefficients versus the PA concentrations (data not shown). The obtained uptake coefficient of $5.4 \cdot 10^{-8}$ corresponds to the extremely low PA concentrations (in the nM range) that occur at the ocean surface. The obtained value can be used to estimate the ozone deposition velocity (υ_d, in m s^{-1}) on the ocean surface at low wind speed. In this regime the deposition velocity of ozone reaches a constant value that is governed by chemical processes at the air-water interface [8]. According to our experimental conditions, the deposition velocity of ozone due to the chemical reactions at the ocean surface at low wind speed can be expressed as follows:

The estimated deposition velocity of ozone for nM-range PA concentrations is $9.7 \cdot 10^{-4}$ m s^{-1}, which is in the same order of magnitude as the upper-limit ozone deposition velocity due to the reaction with chlorophyll ($1 \cdot 10^{-5}$ to $1 \cdot 10^{-3}$ m s^{-1}) [8] and higher than the deposition velocity of $1.2 \cdot 10^{-4}$ m s^{-1} assessed for the reaction of ozone with a mixture of DOM and iodide at typical oceanic concentrations [60]. The value of $9.7 \cdot 10^{-4}$ m s^{-1} determined for the chemical ozone deposition velocity assisted by PA lies in the higher part of the range of ozone deposition velocities measured at the sea ($1.0 \cdot 10^{-4}$ – $1.0 \cdot 10^{-3}$ m s^{-1}) (Fairall et al., 2007). It has to be noted that the deposition velocities measured at the sea combine both, the chemical (reactivity)

and physical (e.g. wind speed, turbulence) effects. Therefore, the surface reaction between ozone and PA has full potential to make an important contribution to the ozone deposition velocity at the ocean surface. Considering that PA is only one example of the dicarboxylic acids that partition at the air-sea interface, the total uptake of ozone on dicarboxylic acids can significantly increase the deposition velocity of ozone at the sea surface.

The data obtained in this study can improve the global climate–chemistry models [57] of the ozone budget in the marine boundary layer of the atmosphere, close to the ocean surface.

References:

1. Engel, A.; Bange, H. W.; Cunliffe, M.; Burrows, S. M.; Friedrichs, G.; Galgani, L.; Herrmann, H.; Hertkorn, N.; Johnson, M.; Liss, P. S.; Quinn, P. K.; Schartau, M.; Soloviev, A.; Stollel, C.; Upstill-Goddard, R. C.; van Pinxteren, M.; Zäncker, B. The Ocean's Vital Skin: Toward an Integrated Understanding of the Sea Surface Microlayer. *Front. Mar. Sci*. **2017**, *30*.
2. Whitehead, J. D.; McFiggans, G.; Gallagher, M. W.; Flynn, M. J. Simultaneous coastal measurements of ozone deposition fluxes and iodine-mediated particle emission fluxes with subsequent CCN formation. *Atmos. Chem. Phys*. **2010**, *10*.
3. **Chang, W.; Heikes, B. G.; Lee, M. Ozone deposition to the sea surface: chemical enhancement and wind speed dependence. *Atmos. Environ*. 2004, *38*.**
4. Gallagher, M. W.; Beswick, K. M.; Coe, H. Ozone deposition to coastal waters. *Quart. J. Royal Met. Soc*. **2001**, *127* (572).
5. Hunt, S. W., Roeselova, M.; Wang, W.; Wingen, L. M.; Knipping, E. M.; Tobias, D. J.; Dabdub, D.; Finlayson-Pitts, B. J. Formation of Molecular Bromine from the Reaction of Ozone with Deliquesced NaBr Aerosol: Evidence for Interface Chemistry. *J. Phys, Chem. A*. **2004**, *108* (52).
6. Liu, Q.; Schurter, L. M.; Muller, C. E.; Aloisio, S.; Francisco, J.S.; Margerum, D. W. Kinetics and Mechanisms of Aqueous Ozone Reactions with Bromide, Sulfite, Hydrogen Sulfite, Iodide, and Nitrite Ions. *Inorg. Chem*. **2001**, *40*.
7. Oldridge, N. W.; Abbatt, J. P. D. Formation of gas-phase bromine from interaction of ozone with frozen and liquid NaCl/NaBr solutions: Quantitative separation of surficial chemistry from bulk-phase reaction. *J. Phys. Chem. A*. **2011**, *115*.

8. Clifford, D.; Donaldson, D. J.; Brigante, M.; D'Anna, B.; George, C. Reactive uptake of ozone by chlorophyll at aqueous surfaces. **2008**, *42* (4).

9. Liss, P. S.; Duce, R. A. *The Sea Surface and Global Change*; Cambridge University Press: Cambridge, U.K., **1997**.

10. Xianliang, Z.; Mapper, K. Photochemical production of low-molecular-weight carbonyl compounds in seawater and surface microlayer and their air-sea exchange. *Mar. Chem.* **1997**, *56*.

11. Steinberg, S. M.; Bada, J. L. Oxalic, glyoxalic and pyruvic acids in eastern Pacific Ocean waters. *J. Mar. Res.* **1984**, *42* (3).

12. Kieber, D. J.; Mopper, K. Photochemical formation of glyoxylic and pyruvic acids in seawater. *Mar. Chem.* **1987**, *21*.

13. Khan, I; Brimblecombe, R.; Clegg, S. L. Solubilities of Pyruvic Acid and the Lower (C1-C6) Carboxylic Acids. Experimental Determination of Equilibrium Vapour Pressures Above Pure Aqueous and Salt Solutions. *J. Atmos. Chem.* **1995**, *22*.

14. Kawamura, K.; Sakaguchi, F. Molecular distributions of water soluble dicarboxylic acids in marine aerosols over the Pacific Ocean including tropics. *J. Geophys. Res. Atmos.* **1999**, *104*.

15. Boreddy, S. K. R.; Kawamura, K.; Tachibana, E. Long-term (2001–2013) observations of water-soluble dicarboxylic acids and related compounds over the western North Pacific: trends, seasonality and source apportionment. *Sci. Rep.* **2017**, *7*.

16. Altieri, K. E., Seitzinger, S. P., Carlton, A. G., Turpin, B. J., Klein, G. C., and Marshall, A. G. Oligomers formed through in-cloud methylglyoxal reactions: Chemical composition, properties, and mechanisms investigated by ultra-high resolution FT-ICR mass spectrometry. *Atmos. Environ.* **2008**, *42*.

17. Romakkaniemi, S.; Kokkola, H.; Smith, J. N.; Prisle, N. L.; Schwier, A. N.; McNeill, V. F.; Laaksonen, A. Partitioning of semivolatile surface‑active compounds between bulk, surface and gas phase. *Geophys. Res. Lett.* **2011**, *38*. **Should be taken out**

18. Reed Harris, A. E.; Pajunoja, A.; Cazaunau, M.; Gratien, A.; Pangui, E.; Monod, A.; Griffith, E. C.; Virtanen, A.; Doussin, J. F.; Vaida, V. Multiphase Photochemistry of Pyruvic Acid under Atmospheric Conditions. *J. Phys. Chem. A.* **2017**, *121*. **Should be taken out**

19. Jammoul, A.; D'Anna, B.; George, C. Photoinduced oxidation of sea salt halides by aromatic ketones: a source of halogenated radicals. *Atmos. Chem. Phys.* **2009**, *9*.

20. Gutzwiller, L.; George, C.; Rolssler, E.; Ammann, M. Reaction Kinetics of NO2 with Resorcinol and 2,7-Naphthalenediol in the Aqueous Phase at Different pH. *J. Phys. Chem. A.* **2002**, *106*.

21. Barcellos da Rosa, M.; Behnke, W.; Zetzsch, C. Study of the heterogeneous reaction of O_3 with CH_3SCH_3 using the wetted-wall flowtube technique. *Atmos. Chem. Phys*. **2003**, *3*.

22. Reeser, D.; Jammoul, A.; Clifford, D.; Brigante, M.; D'Anna, B.; George, C.; Donaldson, D. Photoenhanced reaction of ozone with chlorophyll at the sea-water surface. *J. Phys. Chem. A*. **2009**, *113* (6).

23. Lee, M. T.; Brown, M. A.; Kato, S.; Kleibert, A.; Türler, A.; Ammann, M. Competition between Organics and Bromide at the Aqueous Solution−Air Interface as Seen from Ozone Uptake Kinetics and X‑ray Photoelectron Spectroscopy. *J. Phys. Chem. A*. **2015**, *119* (19).

24. Fu, H.; Ciuraru, R.; Dupart, Y.; Passananti, M.; Tinel, L.; Rossignol, S.; Perrier, S.; Donaldson, D. J.; Chen, J.; George, C. Photosensitized production of atmospherically reactive organic compounds at the air/aqueous interface. *J. Am. Chem. Soc*. **2015**, *137* (26).

25. Tinel, L.; Rossignol, S.; Bianco, A.; Passananti, M.; Perrier, S.; Wang, X.; Brigante, M.; Donaldson, D. J.; George, C. Mechanistic Insights on the Photosensitized Chemistry of a Fatty Acid at the Air/Water Interface. *Environ. Sci. Technol*. **2016**, *50*.

26. Leermakers, P. A.; Vesley, G. F. Photolysis of pyruvic acid in solution. *J. Org. Chem.* **1963**, *28* (4).

27. Guzman, M. I.; Colussi, A. J.; Hoffmann, M. R. Photoinduced oligomerization of aqueous pyruvic acid. *J. Phys. Chem. A*. **2006**, *110* (10).

28. Grgic, I.; Nieto-Gligorovski, L. I.; Net, S.; Temime-Roussel, B.; Gligorovski, S.; Wortham, H. Light induced multiphase chemistry of gas-phase ozone on aqueous pyruvic and oxalic acids. *Phys. Chem. Chem. Phys*. **2010**, *12*.

29. Gómez Alvarez, E.; Wortham, H.; Strekowski, R.; Zetzsch, C.; Gligorovski, S. Atmospheric photo-sensitized heterogeneous and multiphase reactions: From outdoors to indoors. *Environ. Sci. Technol.* **2012**, *46*.

30. Griffith, E. C.; Carpenter, B. K.; Shoemaker, R. K.; Vaida, V. Photochemistry of aqueous pyruvic acid. *Proc. Natl. Acad. Sci. U. S. A*. **2013**, *110* (29).

31. Reed Harris, A. E.; Ervens, B.; Shoemaker, R. K.; Kroll, J. A.; Rapf, R. J.; Griffith, E. C.; Monod, A.; Vaida, V. Photochemical kinetics of pyruvic acid in aqueous solution. *J. Phys. Chem. A* **2014**, *118 (37)*, 8505−8516.

32. Rapf, R. J.; Perkins, R. J.; Carpenter, B. K.; Vaida, V. Mechanistic Description of Photochemical Oligomer Formation from Aqueous Pyruvic Acid. *J. Phys. Chem. A*. **2017**, *121*.

33. Rapf, R. J.; Dooley, M. R.; Kappes, K.; Perkins, R. J.; Vaida, V. pH Dependence of the Aqueous Photochemistry of alpha-Keto Acids. *J. Phys. Chem. A*, **2017**, *121* (44). Should be removed

34. Eugene, A. J.; Guzman, M. I. Reactivity of Ketyl and Acetyl Radicals from Direct Solar Actinic Photolysis of Aqueous Pyruvic Acid. *J. Phys. Chem. A.* **2017**, *121*.

35. Mekic, M.; Brigante, M.; Vione, D.; Gligorovski, S. Exploring the ionic strength effects on the photochemical degradation of pyruvic acid in atmospheric deliquescent aerosol particles. *Atmos. Environ.* **2018**, *185*.

36. Shi, Q.; Pan, N.; Long, H.; Cui, D.; Guo, X.; Long, Y.; Chung, K. H.; Zhao, S.; Xu, C.; Hsu C. S. Characterization of middle-temperature gasification coal tar. Part 3: Molecular composition of acidic compounds. *Energy & Fuels*, **2012**, *27(1)*.

37. Jiang, B.; Liang, Y.; Xu, C.; Zhang, J.; Hu, M.; Shi, Q. Polycyclic Aromatic Hydrocarbons (PAHs) in Ambient Aerosols from Beijing: Characterization of Low Volatile PAHs by Positive-Ion Atmospheric Pressure Photoionization (APPI) Coupled with Fourier Transform Ion Cyclotron Resonance. *Environ. Sci. Technol.* **2014**, *48.*

38. Dankwerts, P. V. *Gas-Liquid Reactions*; McGraw-Hill, New York, U.S.A., **1970**.

39. Ammann, M.; Rossler, E.; Strekowski, R.; George, C. Nitrogen dioxide multiphase chemistry: Uptake kinetics on aqueous solutions containing phenolic compounds. *Phys. Chem. Chem.* **2005**, *7*.

40. Finlayson-Pitts, B. J.; Pitts, Jr., J. N. *Chemistry of the Upper and Lower Atmosphere, Theory, Experiments, and Applications*; Academic Press: California, U.S.A., **2000**.

41. Johnson, P. N.; Davis, R. A. Diffusivity of ozone in water. *J. Chem. Eng. Data* **1996**, *41*.

42. Atkins, P.; De Paula, J. *Physical Chemistry*; OXFORD University Press, Oxford, UK, 2014.

43. Behnke, W.; George, C.; Scheer, V. Zetzsch, C. Production and decay of ClNO2 from the reaction of gaseous N2O5 with NaCl solution: bulk and aerosol experiments. *J. Geophys. Res.* **1997**, *102*.

44. Cooney, O. D.; Kim, S-S.; Davis, E. J. Analyses of mass transfer in hemodialyzers for laminar blood flow and homogeneous dialysate. *Chem. Eng. Sci.*, **1974**, *29*.

45. Thomson, R. E.; Emery, W. J. Data a*nalysis Methods in Physical Oceanography Third Edition;* Elsevier: Waltham, U.S.A., 2014.

46. Herrmann, H. Kinetics of Aqueous Phase Reactions Relevant for Atmospheric Chemistry. *Chem. Rev.* **2003**, *103*.

47. Setschenow, M. Uber die Konstitution der Salzlosungen auf Grund ihres Verhaltens zu Kohlensaure. *Z. phys. Chem.* **1889**, *4*.

48. Rischbieter, E.; Stein, H.; Schumpe, A. Ozone solubilities in water and aqueous salt solutions. *J. Chem. Eng. Data.* **2000**, *45*.

49. Schumpe, A. The estimation of gas solubilities in salt solutions. *Chem. Eng. Sci.* **1993**, *48* (1).

50. Weisenberger, S.; Schumpe, A. Estimation of Gas Solubilities in Salt Solutions from 273 K to 363 K. *AIChE J.* **1996**, *42* (1).

51. Beltran, F. J. *Ozone reaction kinetics for water and wastewater systems*; CRC Press LLC: Florida, U.S.A., **2004**.

52. Larson, R. A.; Weber, E. J. *Reaction mechanisms in environmental organic chemistry*; CRC Press, Florida, U.S.A., **1994**.

53. Schöne, L.; Herrmann, H. Kinetic measurements of the reactivity of hydrogen peroxide and ozone towards small atmospherically relevant aldehydes, ketones and organic acids in aqueous solutions. *Atmos. Chem. Phys.* **2014**, *14*.

54. Naumov, S.; von Sonntag, C. The reactions of bromide with ozone towards bromate and the hypobromite puzzle: A density functional theory study. *Ozone: Sci. Engineer.* **2008**, *30*.

55. Reeser, D. I.; George, C.; Donaldson, D. J. Photooxidation of halides by chlorophyll at the air-salt water interface. *J. Phys. Chem. A.* **2009**, *113*.

56. William Kew, W.; Blackburn, J. W. T.; Clarke, D. J.; Uhrin, D. Interactive van Krevelen diagrams - Advanced visualization of mass spectrometry data of complex mixtures. *Rapid Commun. Mass Spectrom.* **2017**, *31*.

57. Luhar, A. K.; Galbally, I. E.; Woodhouse, M. T.; Thatcher, M. An improved parameterisation of ozone dry deposition to the ocean and its impact in a global climate–chemistry model. *Atmos. Chem. Phys.*, **2017**, *17*.

58. Heikes, B., Lee, M.; Jacob, D.; Talbot, R.; Bradshaw, J.; Singh, H.; Blake, D.; Anderson, B. Fuelberg, H.; Thompson, A. Ozone, hydroperoxides, oxides of nitrogen, and hydrocarbon budgets in the marine boundary layer over the South Atlantic. *J. Geophys. Res.* **1996**, *101* (24).

59. **Chang, W.; Heikes, B. G.; Lee, M. Ozone deposition to the sea surface: chemical enhancement and wind speed dependence. *Atmos. Environ*. 2004, *38*.**

60. Martino, M.; Leze, B.; Baker, A. R.; Liss, P. S. Chemical controls on ozone deposition to water. *Geophys. Res. Letters.* **2012**, *39*.

61. Wang, H.; Lyu X.; Guo, H.; Wang, Y.; Zou, S.; Ling, Z.; Wang, X.; Jiang, F.; Zeren, Y.; Pan, W.; Huang, X.; Shen, J. Ozone pollution around a coastal region of South China Sea: interaction between marine and continental air. *Atmos. Chem. Phys.* **2018**, *18*.

New references

M. I. Guzmán, A. J. Colussi*, and M. R. Hoffmann, Photoinduced Oligomerization of Aqueous Pyruvic Acid. J. Phys. Chem. A, 2006, 110 (10), pp 3619–3626. DOI: 10.1021/jp056097z.

Marcelo I. Guzmán, A. J. Colussi*, and Michael R. Hoffmann, Photogeneration of Distant Radical Pairs in Aqueous Pyruvic Acid Glasses. J. Phys. Chem. A, 2006, 110 (3), pp 931–935. DOI: 10.1021/jp053449t.

Sha-Sha Xia, Alexis J. Eugene, and Marcelo I. Guzman, Cross Photoreaction of Glyoxylic and Pyruvic Acids in Model Aqueous Aerosol. J. Phys. Chem. A, J. Phys. Chem. A, 2018, 122 (31), pp 6457–6466

von Glasow, R., Crutzen, P. J., Heinrich, D. H., and Karl, K. T.: Tropospheric Halogen Chemistry, in: Treatise on Geochemistry, Pergamon, Oxford, 1–67, 2003.

Lucy J. Carpenter*,† and Philip D. Nightingale, Chemistry and Release of Gases from the Surface Ocean, Chem. Rev., 2015, 115 (10), pp 4015–4034.

Angela G. Rincon, Marcelo I. Guzman,† M. R. Hoffmann, and A. J. Colussi, Thermochromism of Model Organic Aerosol Matter, J. Phys. Chem. Lett. 2010, 1, 368–373

Elizabeth A. Pillar†, Marcelo I. Guzman*†, and Jose M. Rodriguez‡, Conversion of Iodide to Hypoiodous Acid and Iodine in Aqueous Microdroplets Exposed to Ozone, Environ. Sci. Technol., 2013, 47 (19), pp 10971–10979.

Marcelo I. Guzman*†, Richa R. Athalye†, and Jose M. Rodriguez‡, Concentration Effects and Ion Properties Controlling the Fractionation of Halides during Aerosol Formation, J. Phys. Chem. A, 2012, 116 (22), pp 5428–5435.

Hansol D. Lee†, Armando D. Estillore‡# , Holly S. Morris†, Kamal K. Ray†, Aldair Alejandro†, Vicki H. Grassian*‡§ , and Alexei V. Tivanski*†, Direct Surface Tension Measurements of

Individual Sub-Micrometer Particles Using Atomic Force Microscopy, J. Phys. Chem. A, 2017, 121 (43), pp 8296–8305.

Annmarie G. Carlton,1 Barbara J. Turpin,1 Ho-Jin Lim,2 Katye E. Altieri,3 and Sybil Seitzinger, Link between isoprene and secondary organic aerosol (SOA): Pyruvic acid oxidation yields low volatility organic acids in clouds, GEOPHYSICAL RESEARCH LETTERS, VOL. 33, L06822, doi:10.1029/2005GL025374, 2006

Katye E. Altieri*†, Annmarie G. Carlton‡, Ho-Jin Lim ‖ , Barbara J. Turpin‡, and Sybil P. Seitzinger, Evidence for Oligomer Formation in Clouds: Reactions of Isoprene Oxidation Products, Environ. Sci. Technol., 2006, 40 (16), pp 4956–4960

Luca Artiglia1,2, Jacinta Edebeli1,3, Fabrizio Orlando1, Shuzhen Chen1,3, Ming-Tao Lee1,4, Pablo Corral Arroyo1,5, Anina Gilgen1,3, Thorsten Bartels-Rausch1, Armin Kleibert 6, Mario Vazdar 7, Marcelo Andres Carignano8, Joseph S. Francisco9, Paul B. Shepson10, Ivan Gladich 8 & Markus Ammann, A surface-stabilized ozonide triggers bromide oxidation at the aqueous solution-vapour interface, NATURE COMMUNICATIONS 2017, ǀ 8: 700 ǀDOI: 10.1038/s41467-017-00823-x

Yao Fu, Yanyan Zhang, Fei Zhang, Jianmin Chen, Zihua Zhu, Xiao-Ying Yu, Does interfacial photochemistry play a role in the photolysis of pyruvic acid in water? Atmospheric Environment 191 (2018) 36–45.